

An Introduction to Discontinuous High-Order Methods

Z.J. Wang (zjwang.com)
Spahr Professor and Chair
Department of Aerospace Engineering
University of Kansas





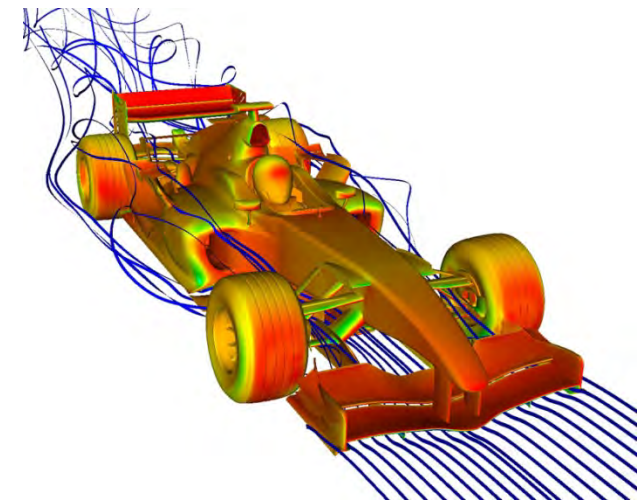
Outline

- Introduction and motivation
- Formulations of discontinuous high-order methods
 - Review of the 1D Godunov finite volume method
 - Different routes to extend the Godunov method to higher-order
 - Further extensions
- Sample applications
 - Implicit LES of transitional flow and flow control
 - Simulations of bio-inspired flows
- Remaining challenges and summary



Introduction – CFD

- ❖ The credibility and usefulness of CFD established over the past two decades;
- ❖ Aerospace industry led the way in CFD development. Auto and other industries became heavy users;
- ❖ CFD is no longer:
 - ❖ Colorful Fluid Dynamics
 - ❖ Continuous Fortran Debugging
 - ❖ Complete Financial Disaster
 - ❖ Constant Frustration and Depression
 - ❖ ...

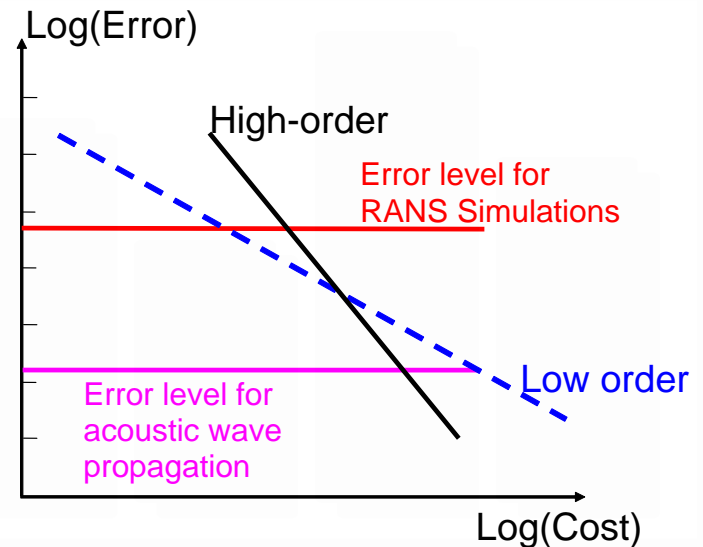
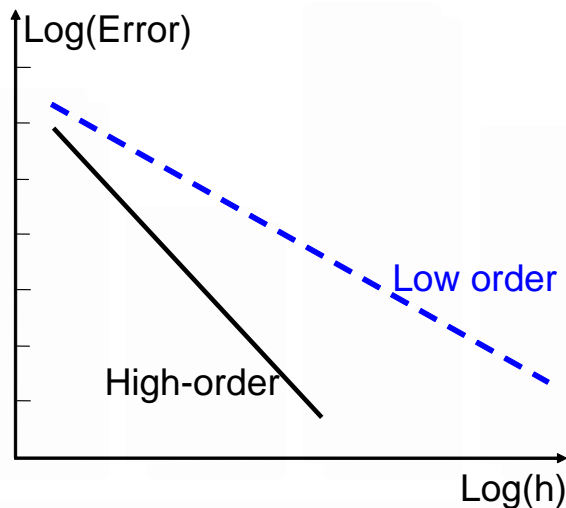




Introduction - High-Order Methods

A method is p-th order accurate if

$$Error \propto h^p$$



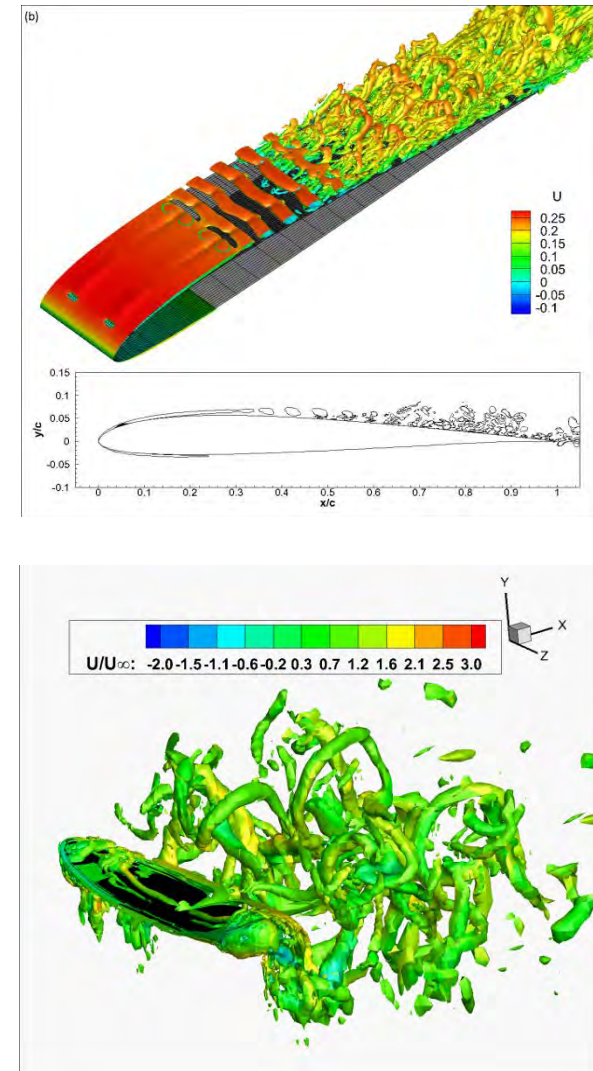
3rd order and higher-order methods are generally called high-order methods in the CFD community

Almost all production and commercial CFD codes use 1st or 2nd-order finite volume methods.



Introduction

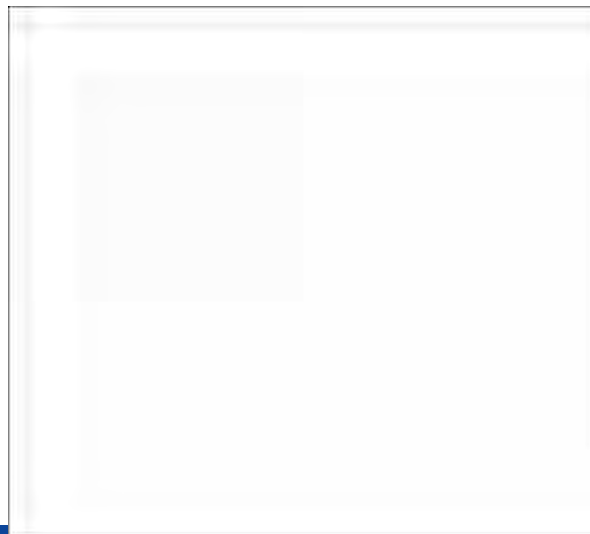
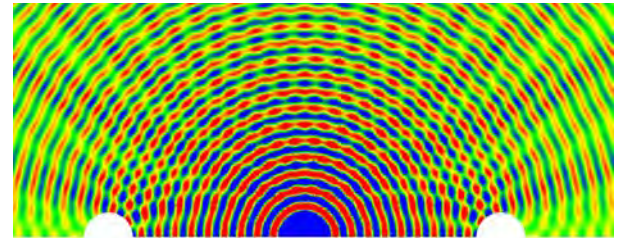
- RANS simulations using 2nd order methods at cruise condition used extensively in aircraft design
- Various hybrid RANS/LES or unsteady RANS approaches demonstrated promise for improved predictions for flow at high-lift configurations
- However, much finer meshes are required for these vortex dominated flows using 2nd order codes



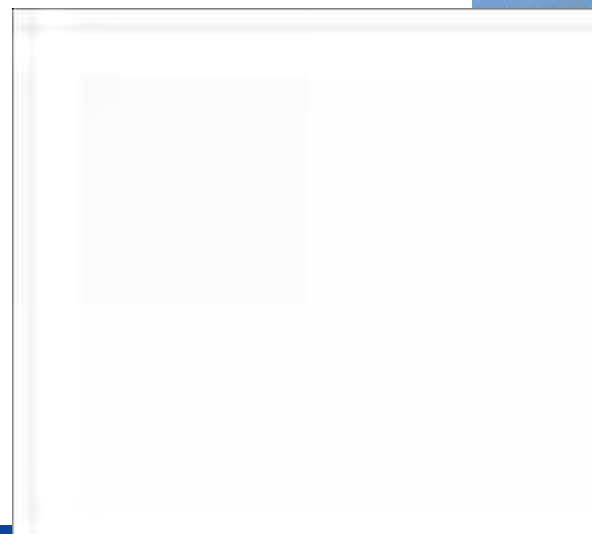


Why High-Order Methods Are Useful

- Aeroacoustic problems
- Vortex dominated flows
- Large eddy simulation (LES) and direct numerical simulation (DNS) of turbulent flow
- ...



2nd Order



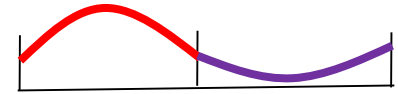
4th Order



Continuous or Discontinuous Methods

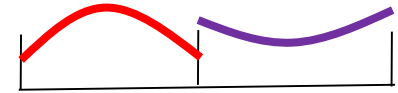
➤ Continuous

- The numerical solution is continuous across cell or element interfaces.
- Examples: residual distribution (RD), streamwise upwind Petrov-Galerkin (SUPG), ...



➤ Discontinuous

- The numerical solution is discontinuous across cell interfaces
- MUSCL/k-exact FV, discontinuous Galerkin (DG), spectral volume/difference (SV/SD), CPR ...

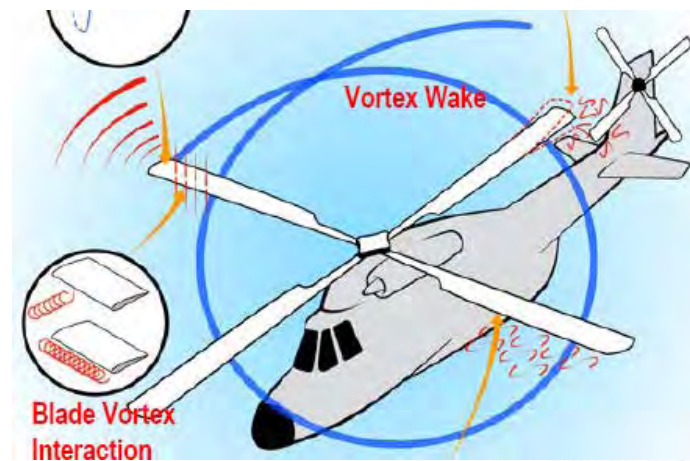


- Both use “upwinding” to account for the wave dynamics of hyperbolic conservation laws



What's Next to Improve Accuracy?

- Further develop 2nd-order codes
 - Improve solution efficiency
 - Employ h-adaptations
 - ...
- Develop higher order methods which can
 - Handle complex geometries
 - Efficient
 - Scalable
 - ...





How to Achieve High-Order Accuracy

- Extend reconstruction stencil 
 - Finite difference, compact
 - Finite volume, ENO/WENO, ...
- Add more internal degrees of freedom 
 - Finite element/spectral element, discontinuous Galerkin
 - Spectral volume (SV)/spectral difference (SD), flux reconstruction (FR) or correction procedure via reconstruction (CPR), ...
- Hybrid approaches 
 - PnPm, reconstructed DG, ...



Extending Stencil vs. More Internal DOFs

- **Simple formulation and easy to understand for structured mesh**
- **Complicated boundary conditions: high-order one-sided difference on uniform grids may be unstable**
- **Boundary conditions trivial with uniform accuracy**
- **Non-uniform and unstructured grids**
 - Reconstruction universal
- **Scalable**
 - Communication through face flux only



Review of Our Related Work

- Came across DG in the mid-1990s.
- Developed a “finite-volume” version of the DG method – spectral volume (SV) in early 2000
- Issues of stability for tetrahedra lead to the development of spectral difference (SD), led by Dr. Yen Liu of NASA Ames, in the mid-2000s
- On simplexes, SD is unstable.
- Flux reconstruction (FR) was developed by Huynh, which we extended to simplex under lifting collocation penalty (LCP). FR & LCP renamed CPR (correction procedure via reconstruction) .



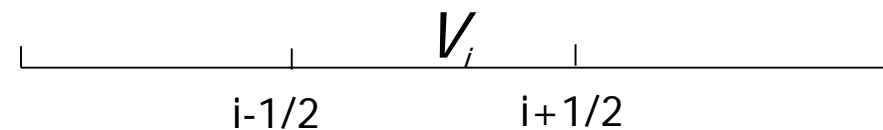
Review of Godunov FV Method

Consider

$$\frac{\partial u}{\partial t} + \frac{\partial f(u)}{\partial x} = 0$$

on domain Ω with proper initial and boundary conditions. Ω is discretized into non-overlapping CVs $\{V_i\}$. Integrating in V_i

$$\int_{V_i} \left(\frac{\partial u}{\partial t} + \frac{\partial f}{\partial x} \right) dx = 0$$





Godunov FV Method (cont.)

We obtain

$$\frac{\partial \bar{u}_i}{\partial t} \Delta x_i + \int_{i-1/2}^{i+1/2} \frac{\partial f}{\partial x} dx = \frac{\partial \bar{u}_i}{\partial t} \Delta x_i + (f_{i+1/2} - f_{i-1/2}) = 0$$

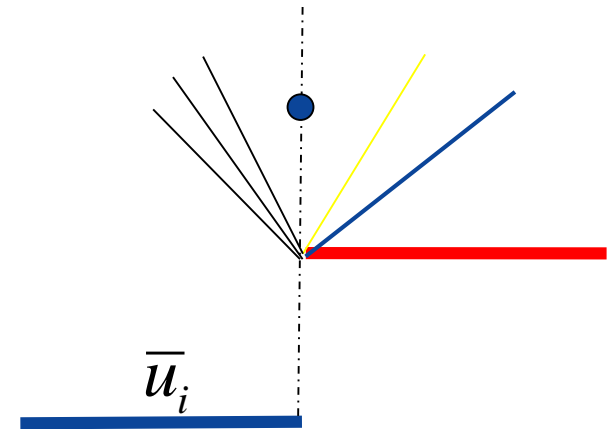
where $\bar{u}_i = \frac{1}{\Delta x_i} \int_{V_i} u dV$

All we need to do is to compute the fluxes at $i+1/2$ and $i-1/2$. However, we only know the cell averaged solutions $\{\bar{u}_i\}$



Godunov FV Method (cont.)

- Assume the solution is piece-wise constant, or a degree 0 polynomial.
- However, a new problem is created. The solution is discontinuous at the interface
- In addition, the obvious solution
$$\hat{f}_{i+1/2} = [f(\bar{u}_i) + f(\bar{u}_{i+1})] / 2$$
is unstable
- A "shock-tube" problem solved to obtain the flux $f(\bullet)$



$i-1/2$

$i+1/2$

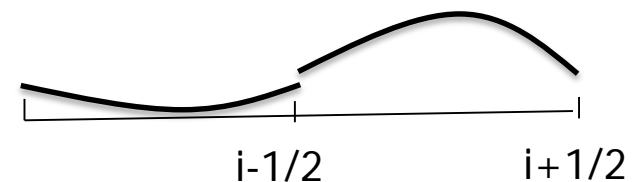


Extension to Higher-Order

- The only way to improve the solution accuracy is to increase the polynomial degree of the solution at each cell
- KEFV, DG, SV and SD methods all degenerate to the Godunov method when $p = 0$!
- To represent a polynomial of higher than $p=0$, multiple DOFs are required, e.g.,

$$u(x) \approx U(x) = a + bx + cx^2 + \dots$$

- These methods differ on how DOFs are defined.





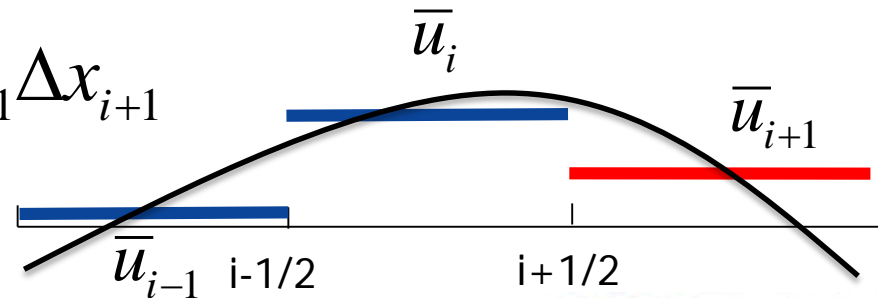
K-Exact Finite Volume Method (MUSCL etc.)

- ❖ Each cell has one DOF \bar{u}_i
- ❖ To build a polynomial with degree higher than 0, neighboring data are used by requiring

$$\int_{V_i} (a + bx + cx^2) dx = \bar{u}_i \Delta x_i$$

$$\int_{V_{i-1}} (a + bx + cx^2) dx = \bar{u}_{i-1} \Delta x_{i-1}$$

$$\int_{V_{i+1}} (a + bx + cx^2) dx = \bar{u}_{i+1} \Delta x_{i+1}$$





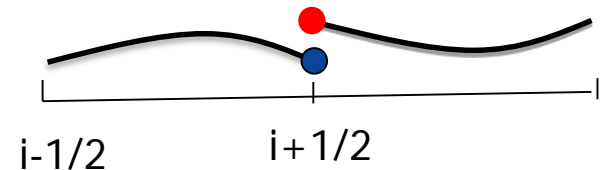
K-Exact Finite Volume Method (cont.)

- ❖ The cell average is updated using a FV method

$$\frac{\partial \bar{u}_i}{\partial t} = - \frac{\hat{f}_{i+1/2} - \hat{f}_{i-1/2}}{\Delta x_i}$$

- ❖ The flux is computed with the reconstructed solutions at the interface from both the left and right cells

$$\hat{f}_{i+1/2} = \hat{f}_{Riem} (U_{i+1/2}^L, U_{i+1/2}^R)$$



e.g.

$$\hat{f}_{i+1/2} = \frac{1}{2} \left[f(U_{i+1/2}^L) + f(U_{i+1/2}^R) - |\alpha| (U_{i+1/2}^R - U_{i+1/2}^L) \right]$$



Discontinuous Galerkin Method

- ❖ Each cell has enough DOFs so that neighboring data are not used in reconstructing a higher-degree polynomial
- ❖ One may choose any DOFs in DG and the method is identical
- ❖ Different DOFs have different numerical property and efficiency
- ❖ Assume we choose a , b and c as the DOFs so that

$$U(x) = a + bx + cx^2$$



Discontinuous Galerkin Method (cont.)

- ❖ However, at each cell we need to update 3 DOFs! How?
- ❖ A weighed residual formulation is used

$$\int_{V_i} 1 * \left(\frac{\partial U}{\partial t} + \frac{\partial f}{\partial x} \right) dx = 0 \quad \text{Finite Volume!}$$

$$\int_{V_i} x * \left(\frac{\partial U}{\partial t} + \frac{\partial f}{\partial x} \right) dx = 0$$

$$\int_{V_i} x^2 * \left(\frac{\partial U}{\partial t} + \frac{\partial f}{\partial x} \right) dx = 0$$



DG Formulation (cont.)

$$\int_{V_i} \varphi^* \left(\frac{\partial U}{\partial t} + \frac{\partial f}{\partial x} \right) dx$$

$$= \frac{\partial}{\partial t} \int_{V_i} \varphi U dx + (\varphi \hat{f})_{i+1/2} - (\varphi \hat{f})_{i-1/2} - \int_{V_i} f \frac{\partial \varphi}{\partial x} dx$$

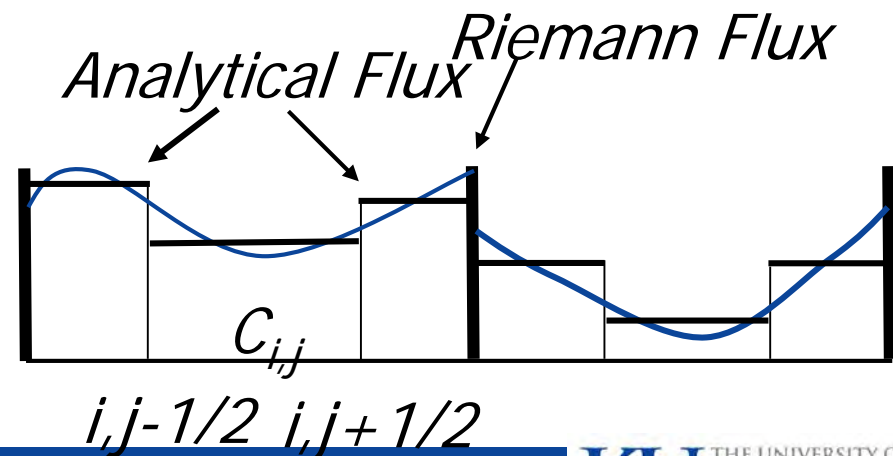
$$= 0$$

At the interfaces $i+1/2$ and $i-1/2$, Riemann fluxes are again used. The volume integral term can be computed using Gauss quadrature.



Spectral Volume Method in 1D

- ❖ Each cell has again enough DOFs so that neighboring data are not used in reconstructing a higher-degree polynomial
- ❖ The DOFs are sub-cell averages. The number of sub-cells is $p+1$ in 1D
- ❖ The polynomial at each cell is reconstructed from the sub-cell averages



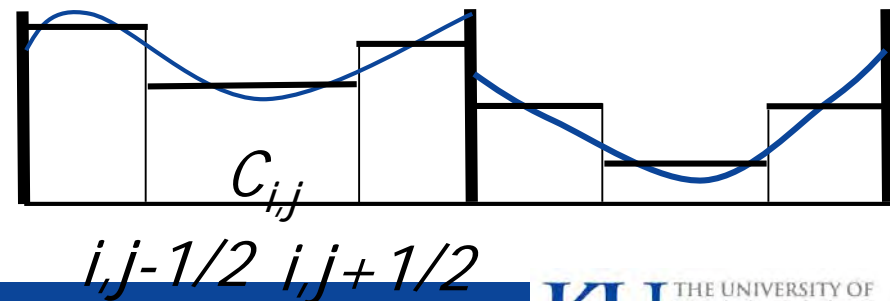


Spectral Volume Method (cont.)

- ❖ The sub-cell averages are updated using a FV method on the sub-cell

$$\frac{d\bar{u}_{i,j}}{dt} \Delta x_{i,j} + (\hat{f}_{i,j+1/2} - \hat{f}_{i,j-1/2}) = 0$$

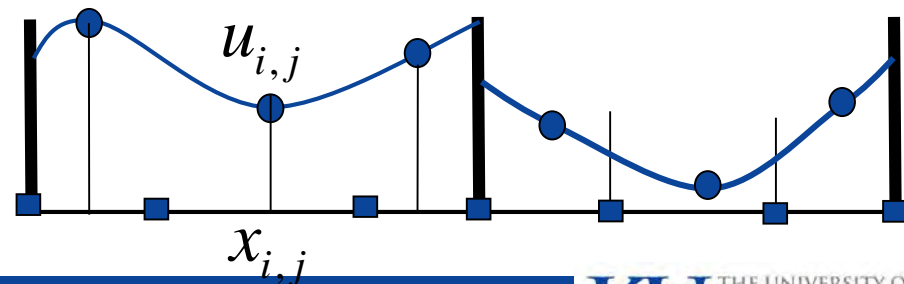
- ❖ Riemann fluxes are only used across the cell interfaces
- ❖ Each cell is partitioned similarly so that they have identical reconstruction formula for non-uniform grids





Spectral Difference Method

- ❖ Each cell has again enough DOFs so that neighboring data are not used in reconstructing a higher-degree polynomial
- ❖ The DOFs are point values at solution points (SP). The number of SP is $p+1$ in 1D
- ❖ The polynomial at each cell is reconstructed from the solutions at the SP using Lagrange interpolation

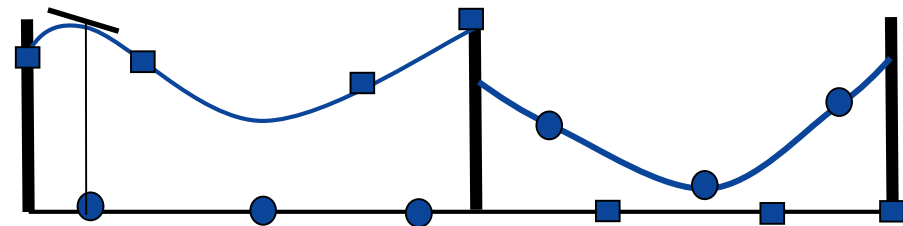




Spectral Difference Method (cont.)

- ❖ In order to update the DOFs, a flux polynomial is built, which is one degree higher than p . A set of flux points are defined
- ❖ Fluxes at the flux points are computed. At the interface, the Riemann flux is again used
- ❖ Let the flux polynomial be $F_i(x)$

$$\frac{du_{i,j}}{dt} + \frac{dF_i(x_{i,j})}{dx} = 0$$





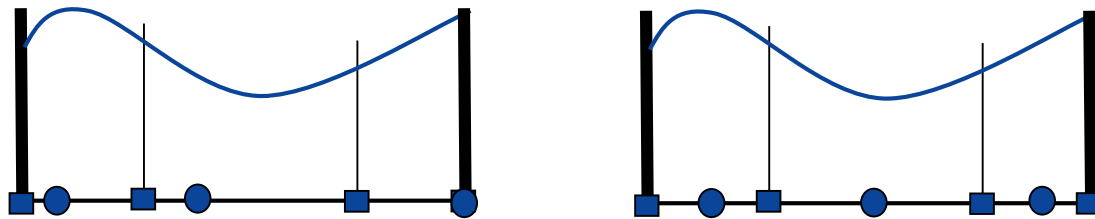
Interesting Results on DG, SV and SD

- ❖ Although DG, SV and SD methods can all achieve $(p+1)$ th order of accuracy, DG has the lowest error magnitude;
- ❖ SV and SD methods allow larger time steps than the DG method (CFL $1/3$ for DG and $1/2$ for SD/SV at second order)
- ❖ The partition in the SV method and the location of the flux points in the SD method strongly affect the stability and accuracy

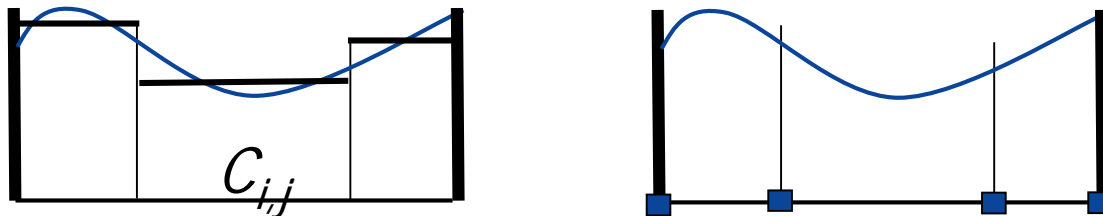


Several Recent "Surprises"

- ❖ The SD scheme only depends on the flux points, independent of the solution points;



- ❖ The 1D SD and SV schemes are identical if the partition points coincide with flux points!





Main Idea of FR (CPR)

We again solve

$$\frac{\partial u}{\partial t} + \frac{\partial f}{\partial x} = 0$$

using a differential formulation

$$\frac{\partial U_i(x)}{\partial t} + \frac{\partial F_i(x)}{\partial x} = 0, \quad U_i(x) \in P^k, \quad F_i(x) \in P^{k+1}$$

The DOFs are solutions at a set of "solution points"



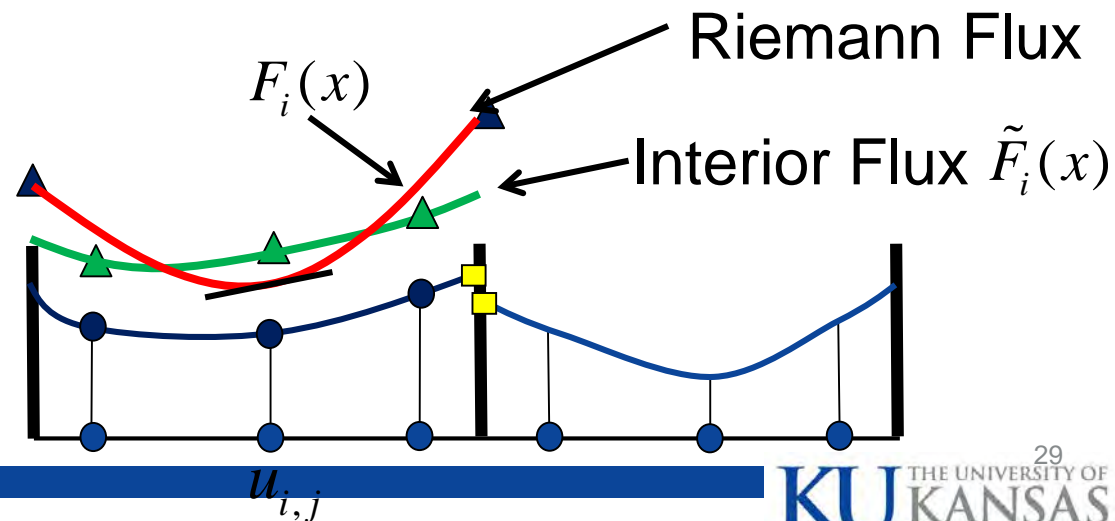
Main Idea of CPR (FR)

Find a flux polynomial $F_i(x)$ one degree higher than the solution, which minimizes

$$\|\tilde{F}_i(x) - F_i(x)\|$$

The use the following to update the DOFs

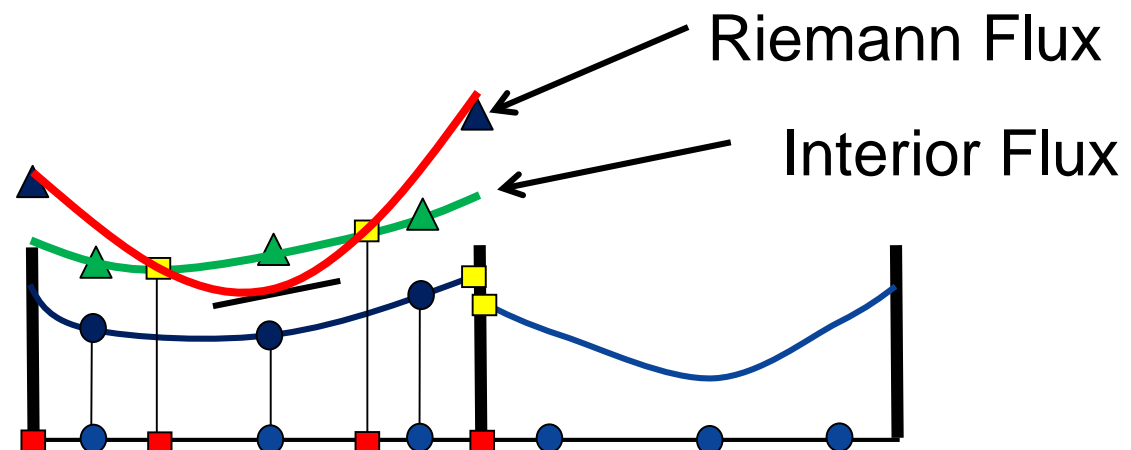
$$\frac{du_{i,j}}{dt} + \frac{dF_i(x_{i,j})}{dx} = 0$$





Connection to Spectral Volume/Difference

- Define a set of flux points, which are used to build a degree $k+1$ flux polynomial
- Compute the flux at the flux points
- At the interfaces use the Riemann flux
- Build a Lagrange flux polynomial





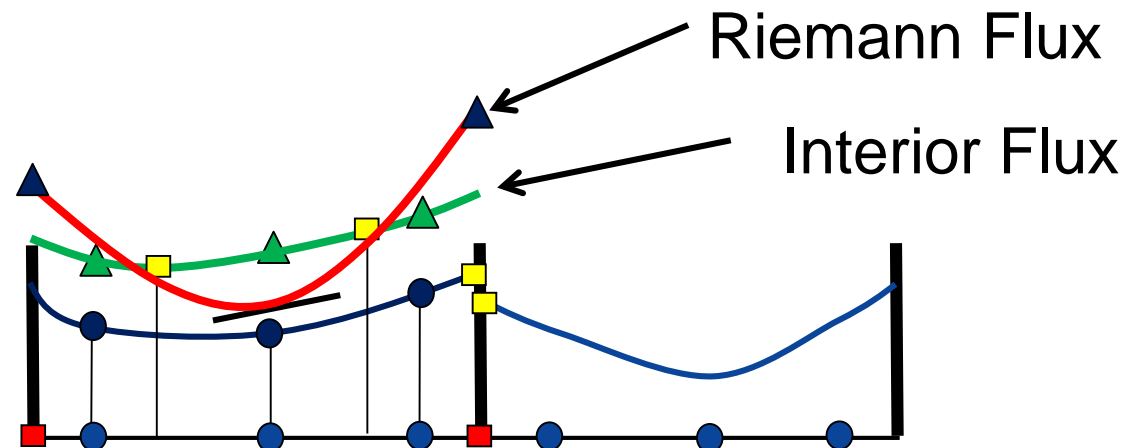
Connection to DG

- If the following equations are satisfied

$$\int_{V_i} [\tilde{F}_i(x) - F_i(x)] dx = 0$$

$$\int_{V_i} [\tilde{F}_i(x) - F_i(x)] x dx = 0$$

- The scheme is DG!





CPR in Multiple Dimensions

Consider

$$\frac{\partial Q}{\partial t} + \nabla \cdot \vec{F}(Q) = 0$$

The weighted residual form is

$$\int_{V_i} \left(\frac{\partial Q}{\partial t} + \nabla \cdot \vec{F}(Q) \right) W dV = \int_{V_i} \frac{\partial Q}{\partial t} W dV + \int_{\partial V_i} W \vec{F}(Q) \cdot \vec{n} dS - \int_{V_i} \nabla W \cdot \vec{F}(Q) dV = 0.$$

Let Q^h be the discontinuous approximate solution in P^k .

The face flux integral replaced by a Riemann flux

$$\int_{V_i} \frac{\partial Q_i^h}{\partial t} W dV + \int_{\partial V_i} W \tilde{F}^n(Q_i^h, Q_{i+}^h, \vec{n}) dS - \int_{V_i} \nabla W \cdot \vec{F}(Q_i^h) dV = 0.$$

Performing integration by parts to the last term

$$\int_{V_i} \frac{\partial Q_i^h}{\partial t} W dV + \int_{V_i} W \nabla \cdot \vec{F}(Q_i^h) dV + \int_{\partial V_i} W \left[\tilde{F}^n(Q_i^h, Q_{i+}^h, \vec{n}) - F^n(Q_i^h) \right] dS = 0.$$



CPR in 2D (cont.)

Introduce the lifting operator

$$\int_{V_i} W \delta_i dV = \int_{\partial V_i} W [\tilde{F}] dS$$

where $\delta_i \in P^k$, $[\tilde{F}] = [\tilde{F}^n(Q_i^h, Q_{i+}^h, \vec{n}) - F^n(Q_i^h)]$ Then we have

$$\int_{V_i} \frac{\partial Q_i^h}{\partial t} W dV + \int_{V_i} W \nabla \cdot \vec{F}(Q_i^h) dV + \int_{\partial V_i} W \delta_i dV = 0,$$

which is equivalent to

$$\frac{\partial Q_i^h}{\partial t} + \nabla \cdot \vec{F}(Q_i^h) + \delta_i = 0.$$

In the new formulation, the weighting function completely disappears! Note that δ_i depends on W .



Lifting Operator – Correction Field

Obviously, the computation of δ_i is the key. From

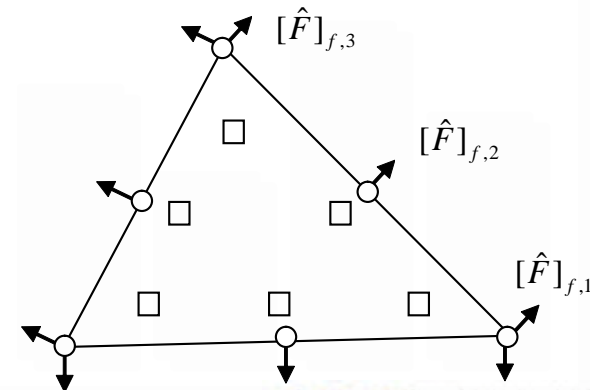
$$\int_{V_i} W \delta_i dV = \int_{\partial V_i} W [\tilde{F}] dS,$$

if $[\tilde{F}], \delta_i \in P^k$ δ_i can be computed explicitly given W. Define a set of “flux points” along the faces, and set of solution points, where the “correction field” is computed as shown.

Then

$$\delta_{i,j} = \frac{1}{|V_i|} \sum_{f \in \partial V_i} \sum_l \alpha_{j,f,l} [\tilde{F}]_{f,l} S_f,$$

$\alpha_{j,f,l}$ lifting coefficients independent of Q



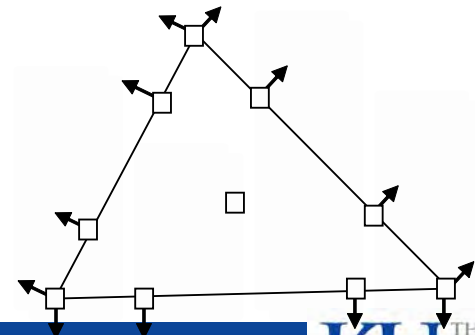
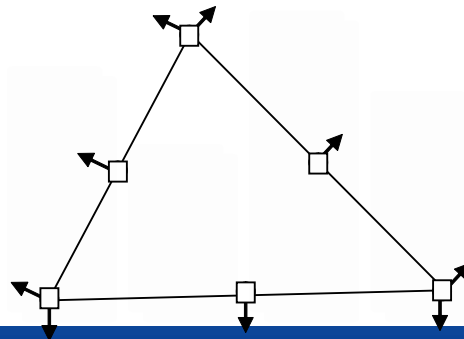


The CPR Formulation (cont.)

Finally the following equation is solved at the solution point j (collocation points)

$$\frac{\partial Q_{i,j}^h}{\partial t} + \nabla \cdot \vec{F}(Q_{i,j}^h) + \frac{1}{|V_i|} \sum_{f \in \partial V_i} \sum_l \alpha_{j,f,l} [\tilde{F}]_{f,l} S_f = 0.$$

The first two terms correspond to the differential equation, and the 3rd term is the “lifting penalty” term, thus the name LCP. If all the flux points coincide with the solution points, the formulation is the most efficient

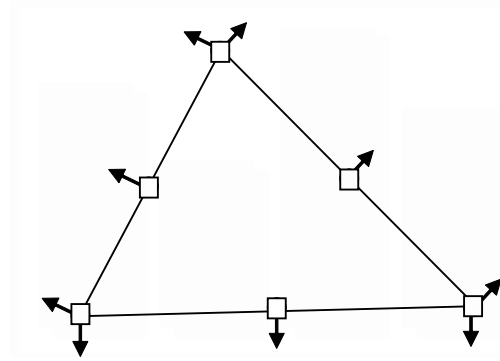




Computation of the Interior Divergence

How to compute the red term?

$$\frac{\partial Q_{i,j}^h}{\partial t} + \nabla \cdot \vec{F}(Q_{i,j}^h) + \frac{1}{|V_i|} \sum_{f \in \partial V_i} \sum_l \alpha_{j,f,l} [\tilde{F}]_{f,l} S_f = 0.$$



➤ Lagrange polynomial (LP)

- Compute the fluxes at the solution points, and then generate Lagrange flux polynomials
- Take the divergence at the solution points

➤ Chain rule (CR)

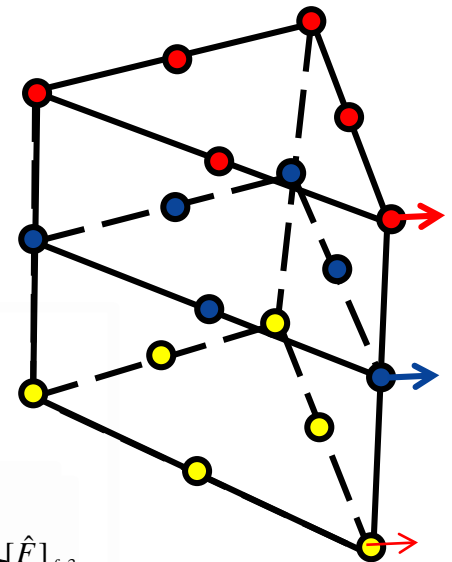
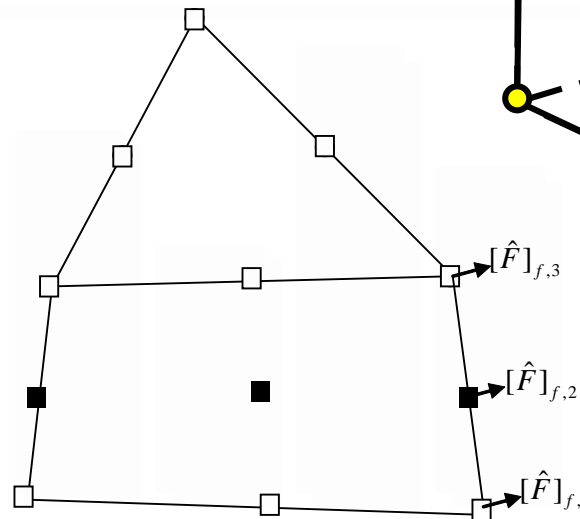
$$\nabla \cdot \vec{F}(Q_i^h) = \frac{\partial F^x(Q_i^h)}{\partial x} + \frac{\partial F^y(Q_i^h)}{\partial y} = \frac{\partial F^x}{\partial Q} \frac{\partial Q_i^h}{\partial x} + \frac{\partial F^y}{\partial Q} \frac{\partial Q_i^h}{\partial y} = \frac{\partial \vec{F}}{\partial Q} \cdot \nabla Q_i^h$$

More accurate!



Mixed Grids

- In order to minimize data reconstruction and communication, solution points coincide with flux points
- For quadrilateral elements, the corrections are one-dimensional!
- Mass matrix is I for all cell-types

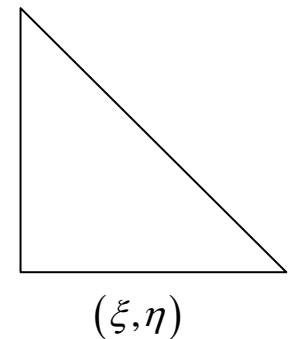
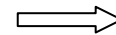
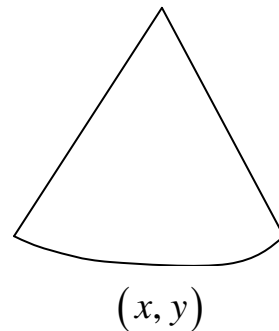




Curved Boundaries

- Transform the governing equations from the (curved) physical domain to the (straight) computational domain;
- The LCP formulation is then applied to the transformed equations in the standard element
- Straightforward!

$$\frac{\partial \tilde{Q}}{\partial t} + \frac{\partial F^\xi}{\partial \xi} + \frac{\partial F^\eta}{\partial \eta} = 0$$

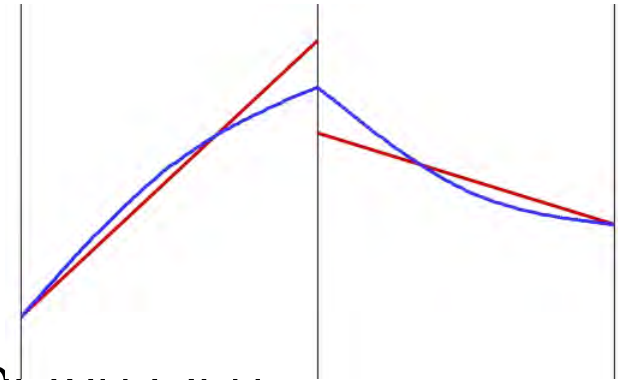




Viscous Flux Computation - Bassi and Rebay II

1-D demonstration

- The common solution at the interface is simply the average of solutions at two sides of the face



$$Q_{f,l}^{com} = \frac{Q_{f,l}^- + Q_{f,l}^+}{2}$$

- The common gradient can be written as the average of the corrected gradients

$$\nabla Q_{f,l}^{com} = \frac{1}{2} (\nabla Q_{f,l}^- + r_{f,l}^- + \nabla Q_{f,l}^+ + r_{f,l}^+)$$



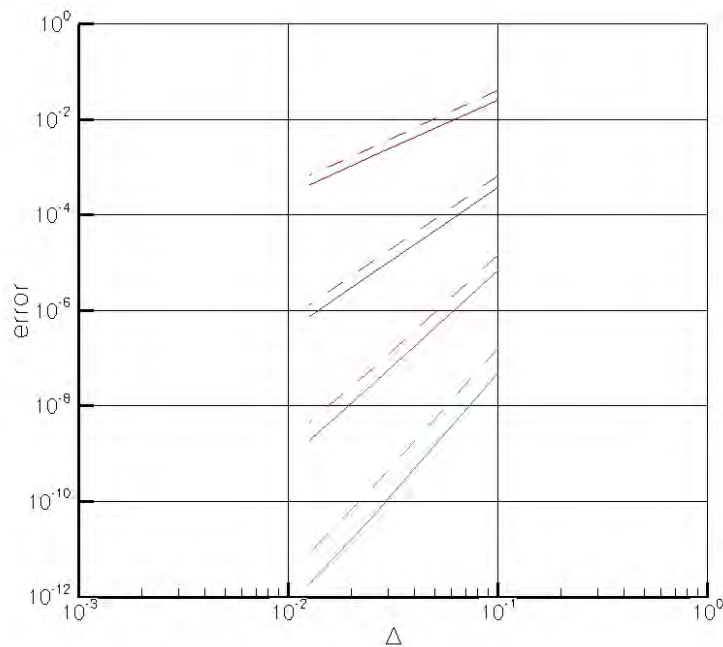
Further Extensions

- Extension to mixed meshes (tets, prisms, ...) and high-order boundaries
- Implicit, p-multigrid and line solvers
- K-exact parameter-free moment limiter
- Perfect matched layer absorbing boundary condition for CAA problems
- Extension to moving boundary problems using dynamic meshes
- Implementation on a cluster of CPUs and GPUs

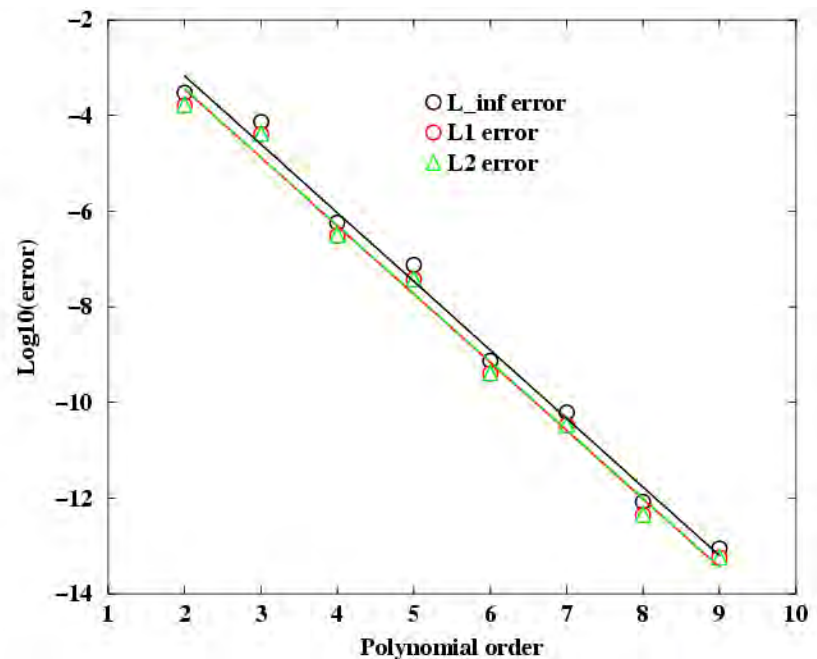


Sample Applications

- Transitional flow over a wing and separation control using surface roughness
- Simulation of bio-inspired flows



h-refinement

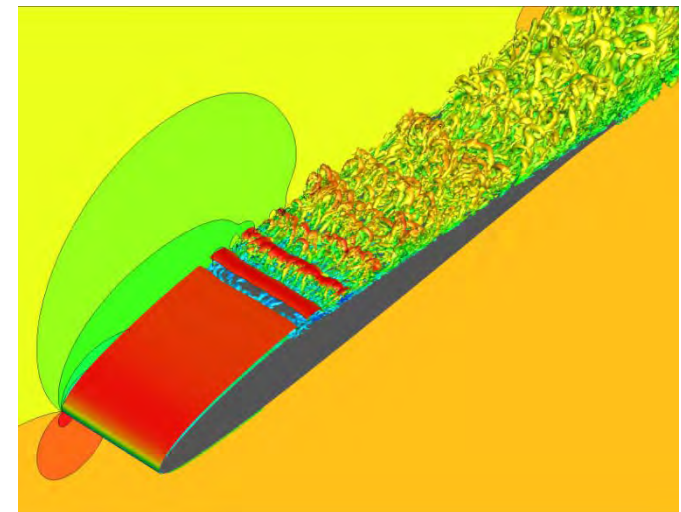
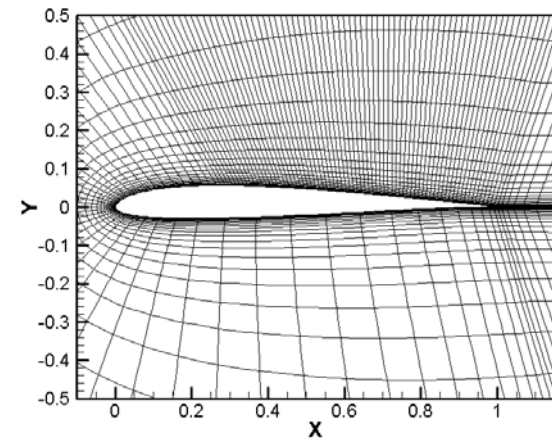


p-refinement



Transitional Flow over SD7003 Wing

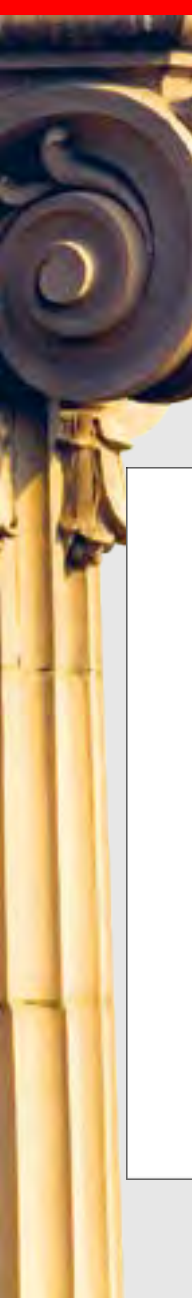
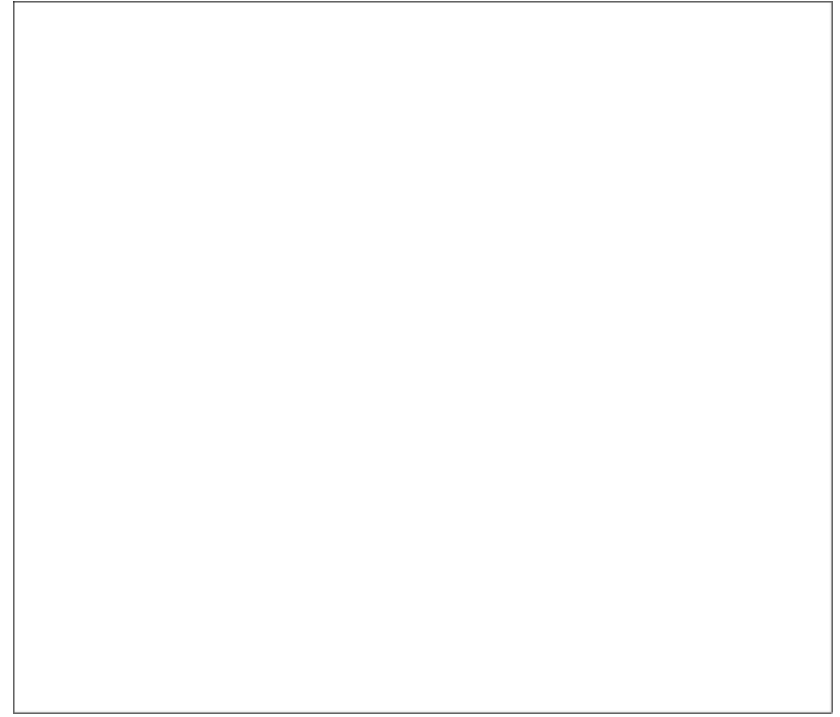
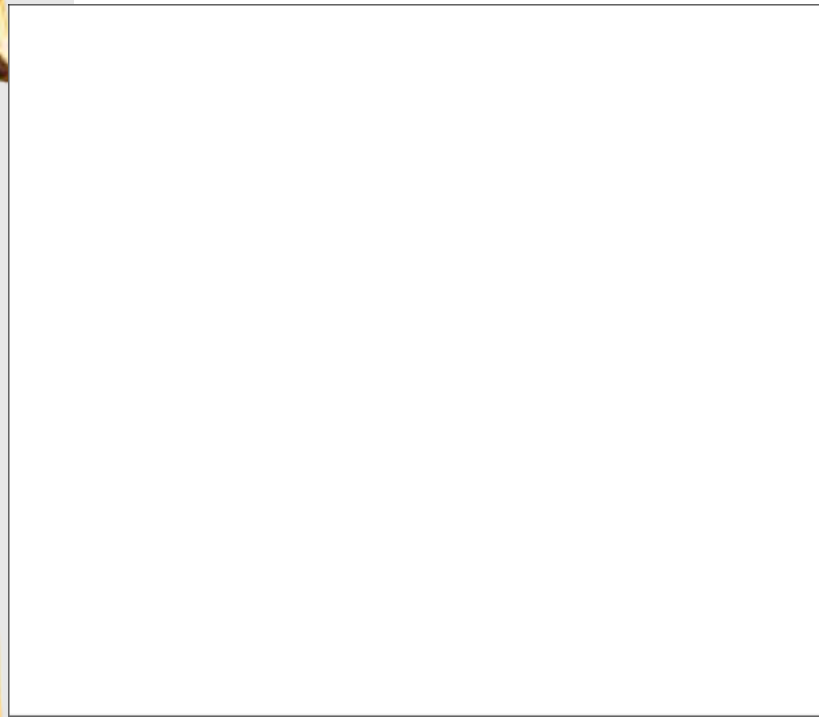
- AOA = 4 deg., $Re = 60,000$
- Spectral difference method
- 253,600 cells, span = 20% c
- No free stream turbulence
- Implicit LES – no SGS model
- 3rd order in time and 3rd and 4th order in space
- Quadratic boundary
- nDOFs/equation
 - 3rd order: 6,847,200
 - 4th order: 16,230,400





Animation of Transition Process

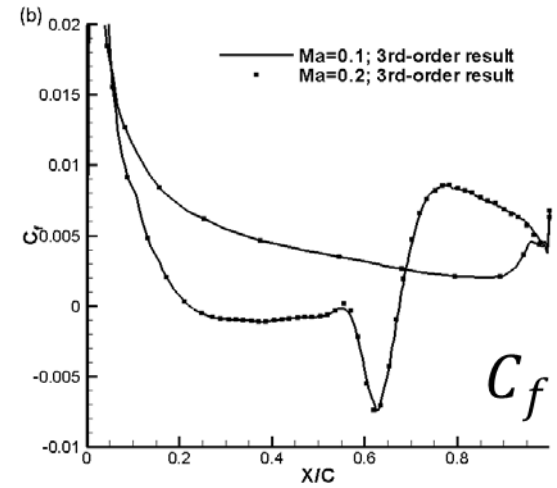
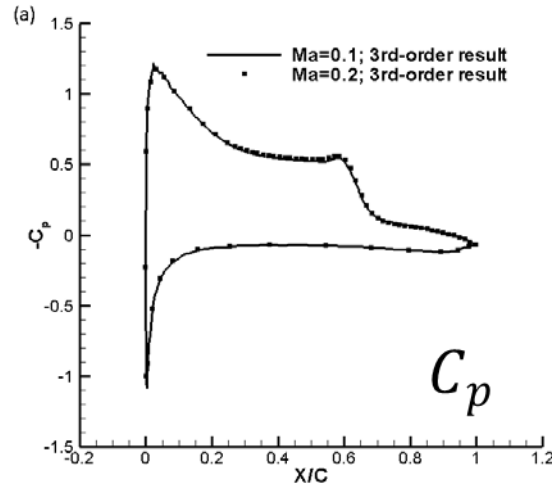
Iso-surfaces of Q-criterion colored by streamwise velocity



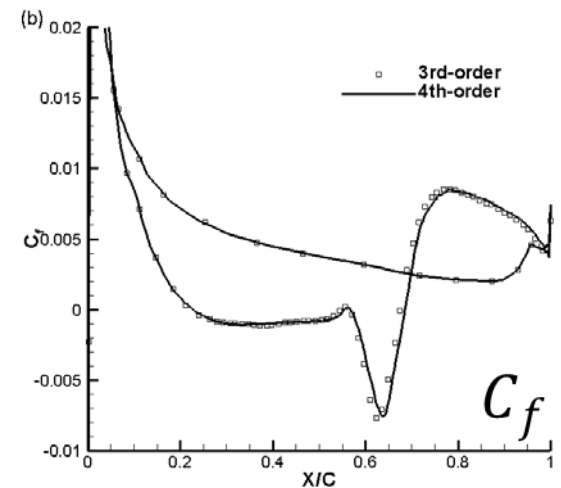
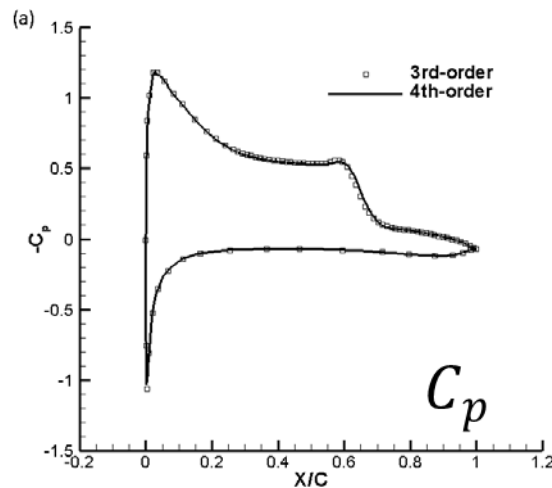


Statistical Results Verification

Mach independent



P-refinement study





Roughness Bumps for Separation Control

W_{AC} Width
 L_{BD} Length
 H_{EF} Height
 X_E Location

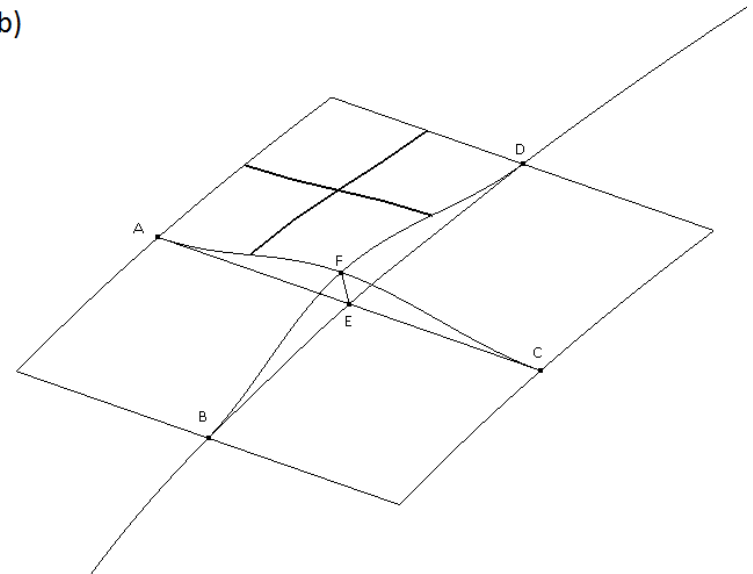
 N_{bump} Number of bumps

C_L Lift coefficient
 C_D Drag coefficient
 C_{Dp} Drag from pressure
 C_{Df} Drag from friction
 L/D Lift-to-drag ratio

(a)



(b)



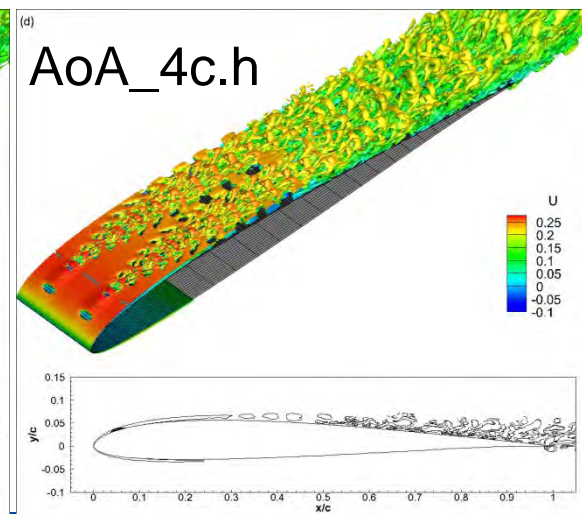
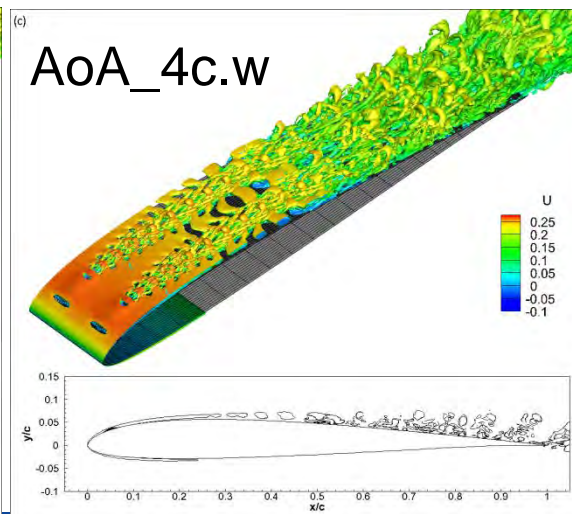
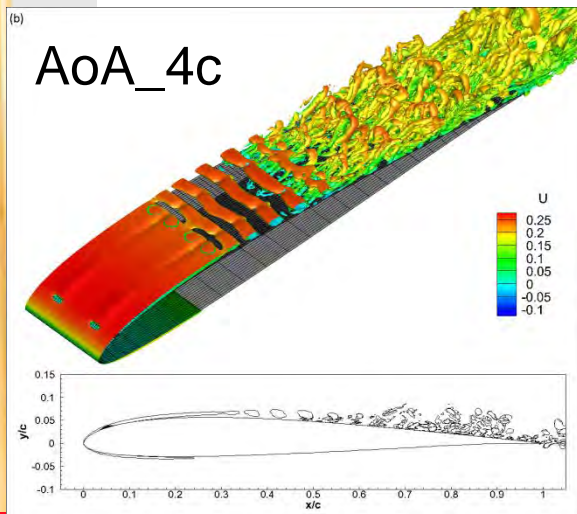
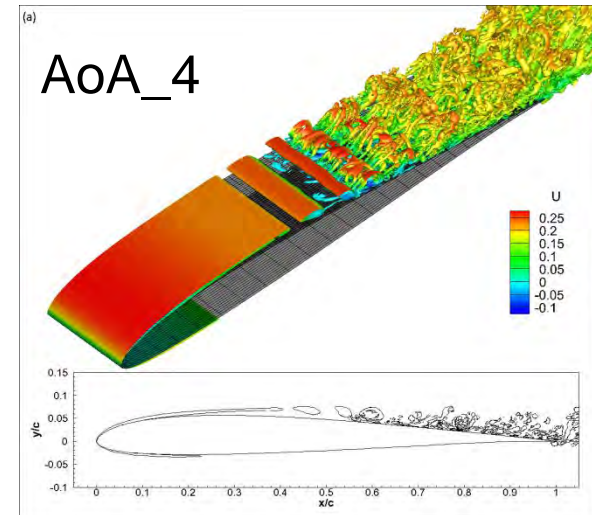


Effects of Bump Size

Table 2. Parameters of the roughness bumps

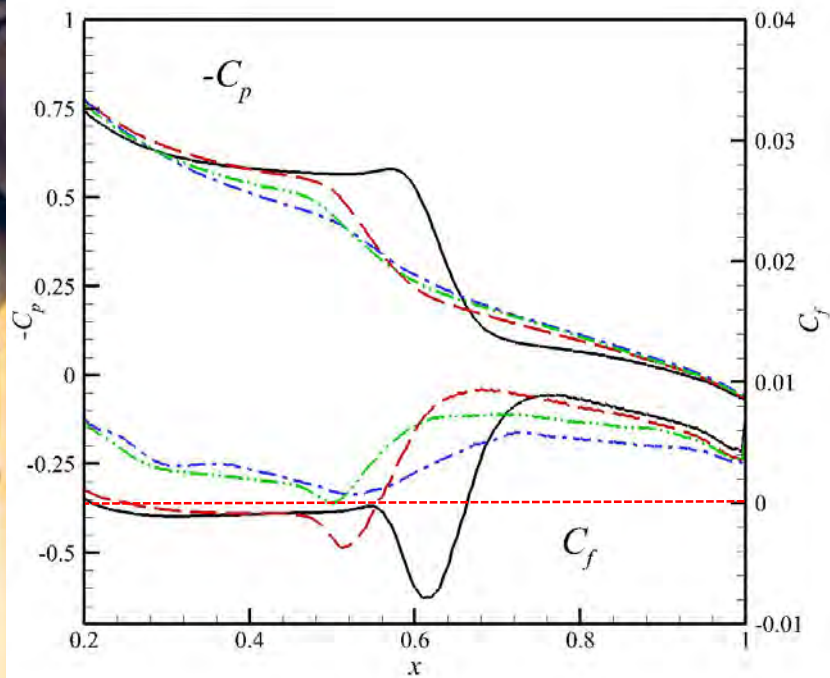
Case	X_E	W_{AC}	L_{BD}	H_{EF}	N_{bump}	δ_E
AoA_4	N/A	N/A	N/A	N/A	N/A	0.0049
AoA_4c	0.05	0.045	0.045	0.0035	2	N/A
AoA_4c.w	0.05	0.090	0.045	0.0035	2	N/A
AoA_4c.h	0.05	0.045	0.045	0.005	2	N/A

Base model
Control
Control-
Control-
h





Flow Control Performance



Case	C_L	C_D	C_{Dp}	C_{Df}	L/D
AoA_4	0.600	2.34e-2	1.38e-2	0.97e-2	25.6
AoA_4c	0.593	2.05e-2	1.00e-2	1.05e-2	28.9
AoA_4c.w	0.579	2.10e-2	0.94e-2	1.16e-2	27.6
AoA_4c.h	0.579	2.07e-2	0.95e-2	1.12e-2	28.0

Summary:

- The LSB is reduced or avoided with roughness bumps. L/D increases 12%.
- Larger and taller bumps generate larger disturbances and trigger earlier vortex breakdown

AoA_4 (solid line)

AoA_4c (dash line)

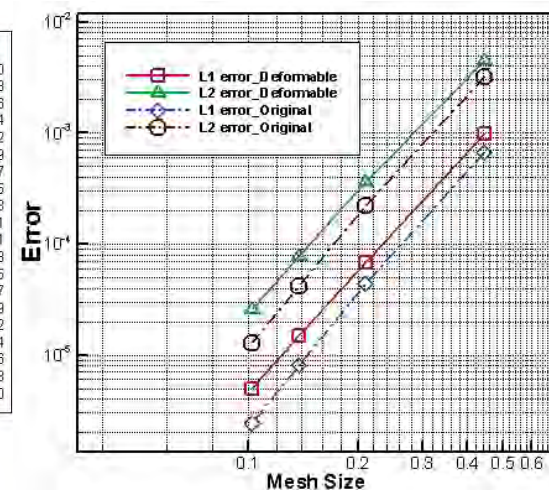
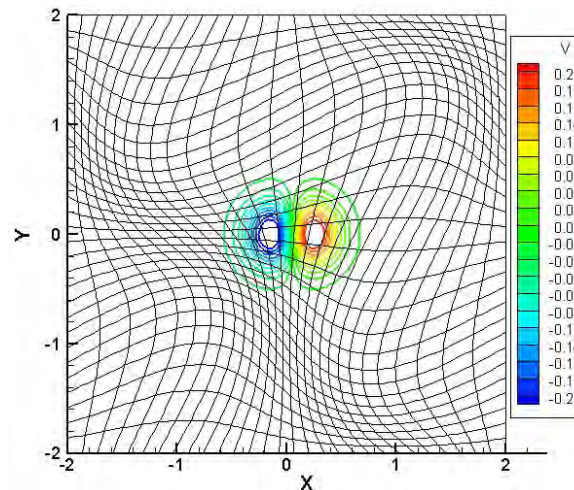
AoA_4c.w (dash-dot line)

AoA_4c.h (dash-dot-dot line)



Simulation of Bio-Inspired Flows

- High-order methods may be more suitable than low order ones because the flow is vortex-dominated
- The solver is extended to handle dynamic meshes
 - Mesh deformation, grid quality issues
 - Geometric conservation law (free-stream preservation)
 - Time accuracy





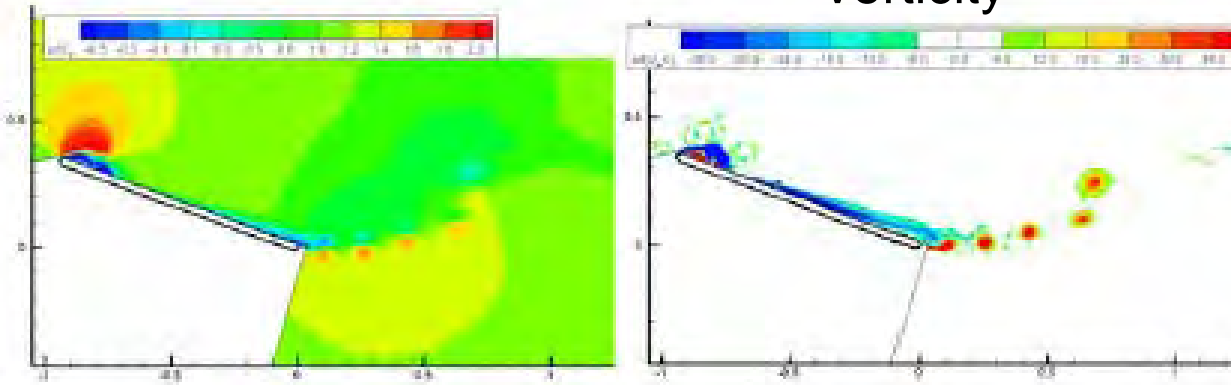
2D Computation – Flat Plate Pitch Motion

$Re = 10,000$, $k = \omega C / (2U) = 0.2$

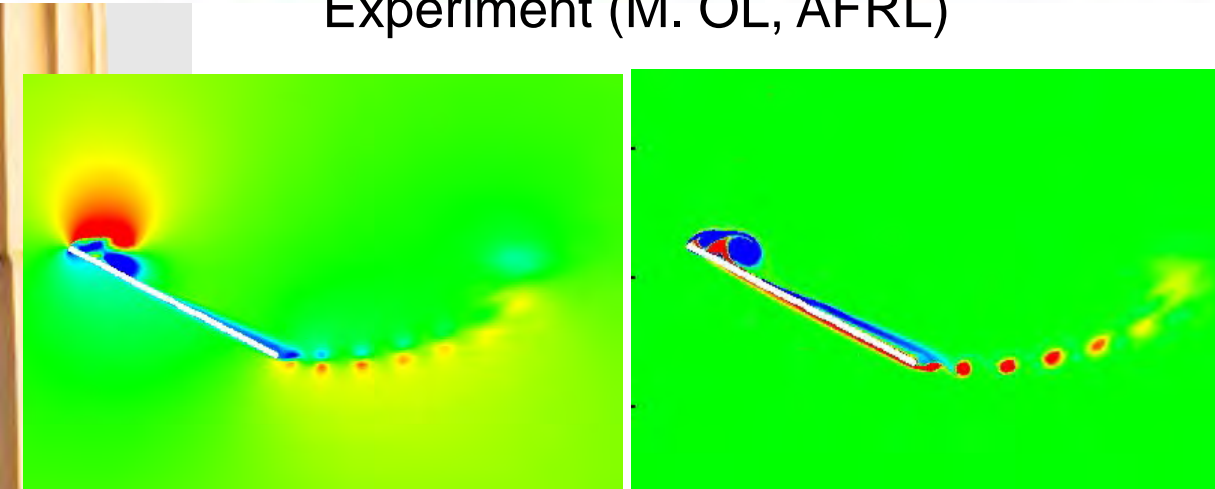
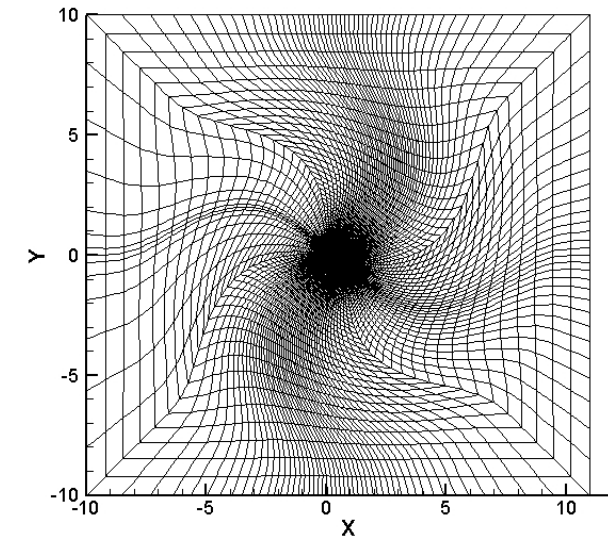
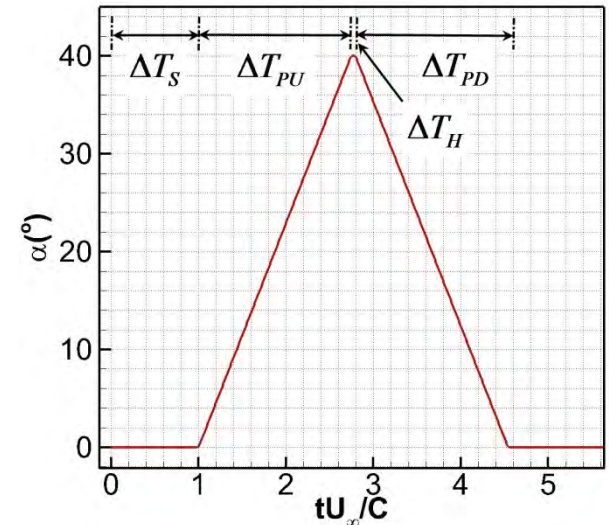


u

Vorticity



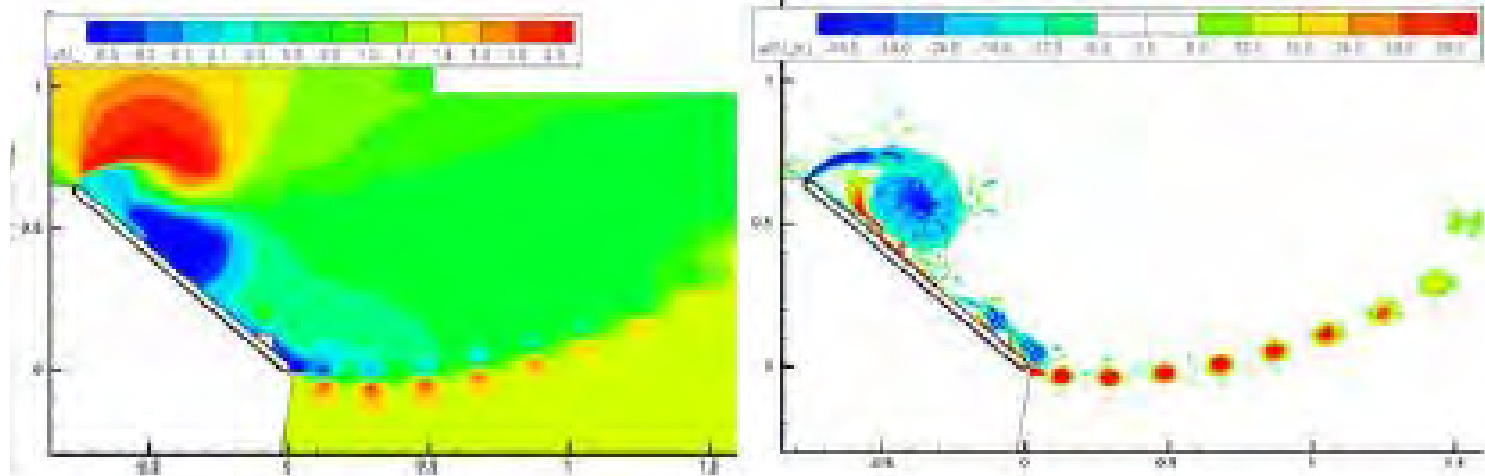
Experiment (M. OL, AFRL)



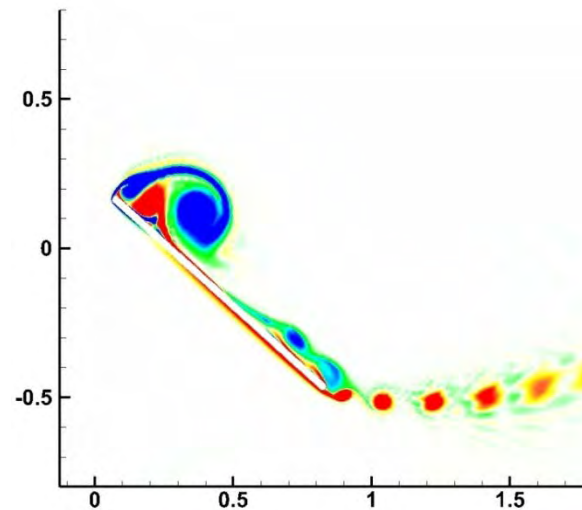
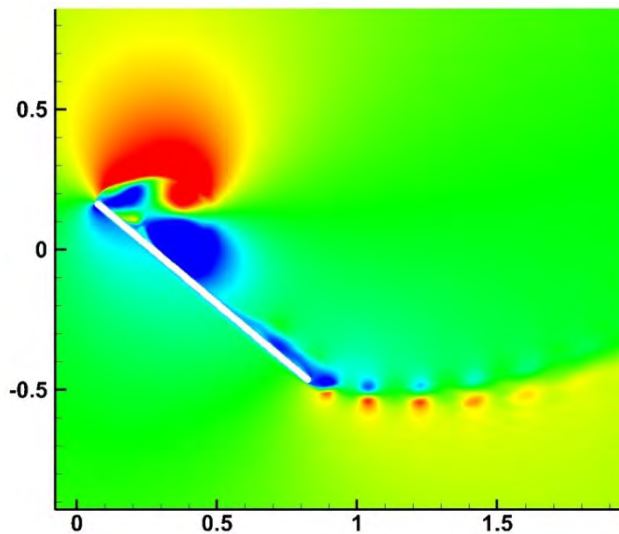
Computation



Comparison with Experimental Results (cont.)



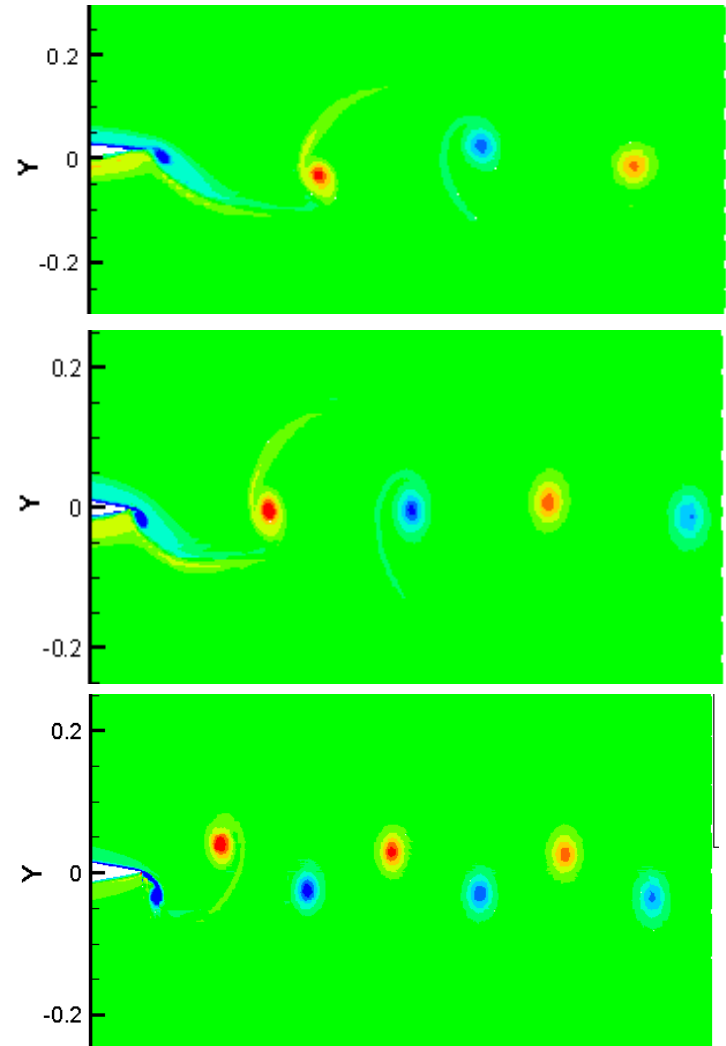
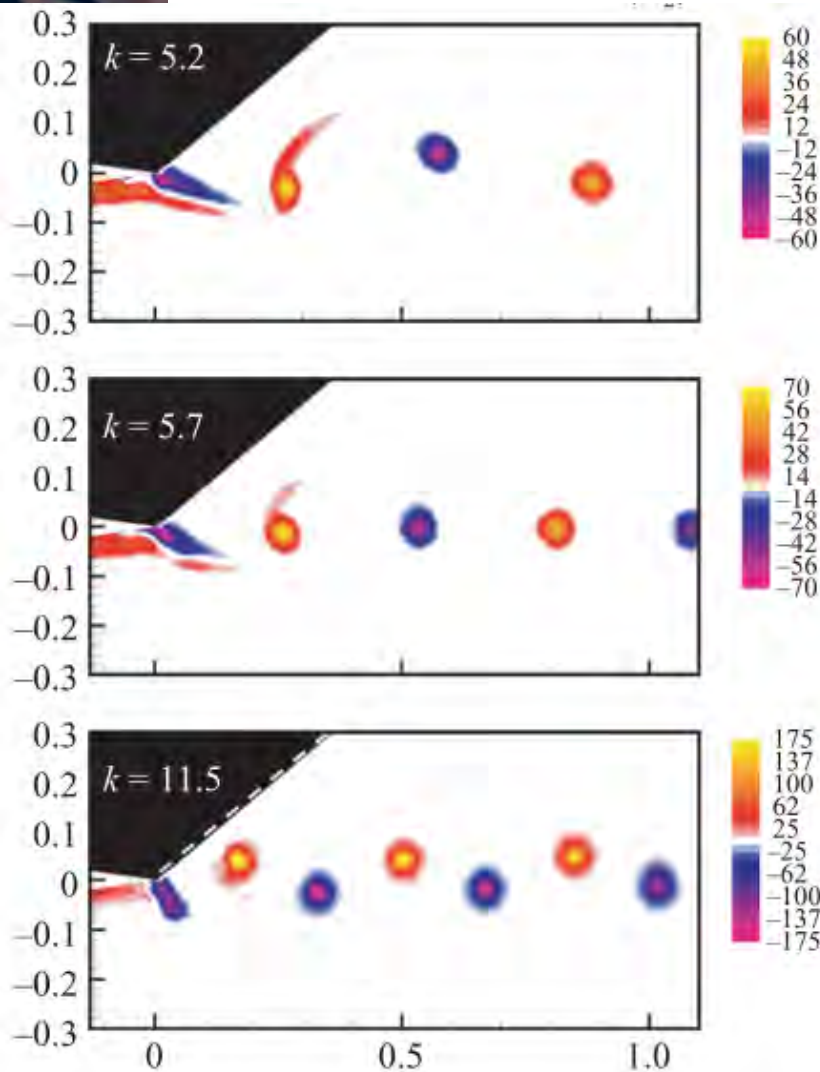
Experiment (M. OL, AFRL)



Computation



Comparison with Experimental Results - Wake



St=0.19

Bohl and
Koochesfhani

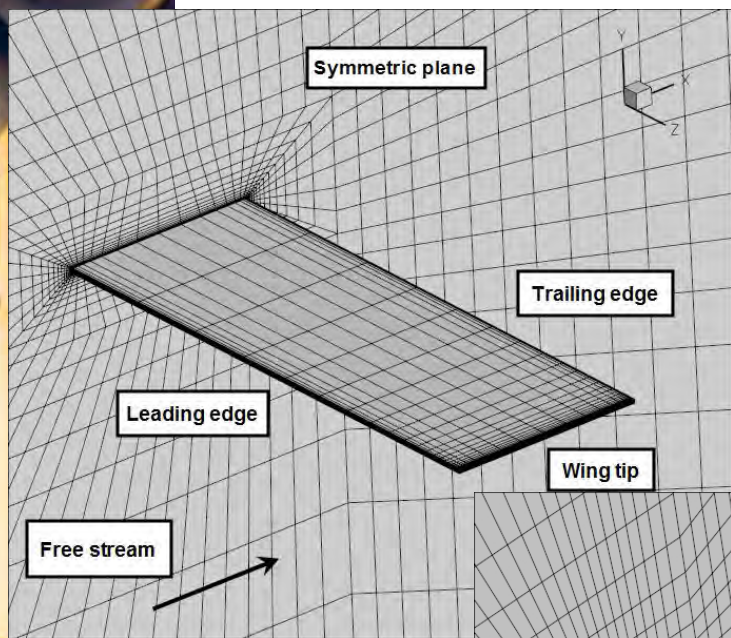
Computatio

n



3D Simulations – Flapping Motion

- Flow Parameters: $Re=1200$, $k=4.5$, $St=0.33$, $AR=2.68$. Experiments performed by Hu group



Rectangular

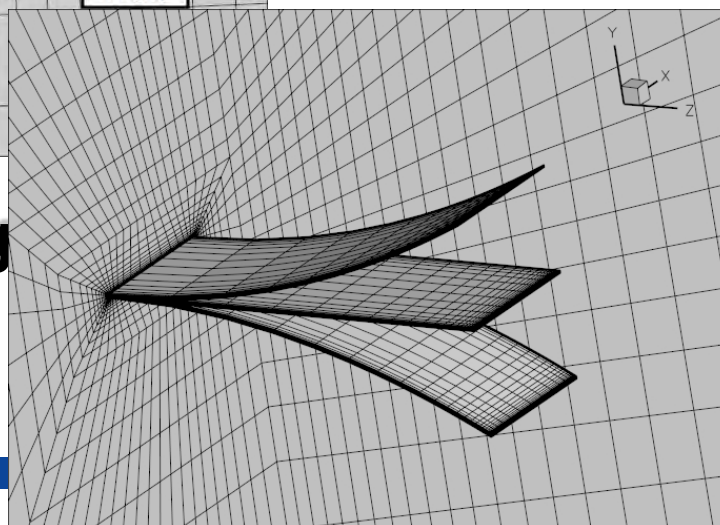


Elliptic



Bio-inspired

Rectangular Wing

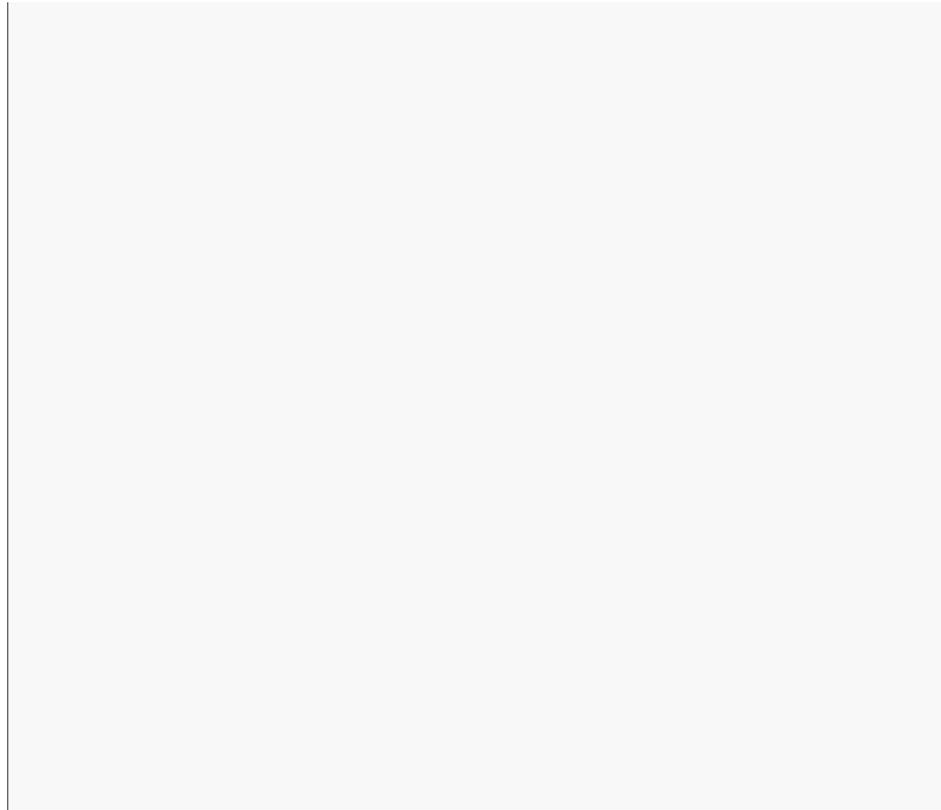


Flapping Motion



3D Simulations – Flapping Motion Movie

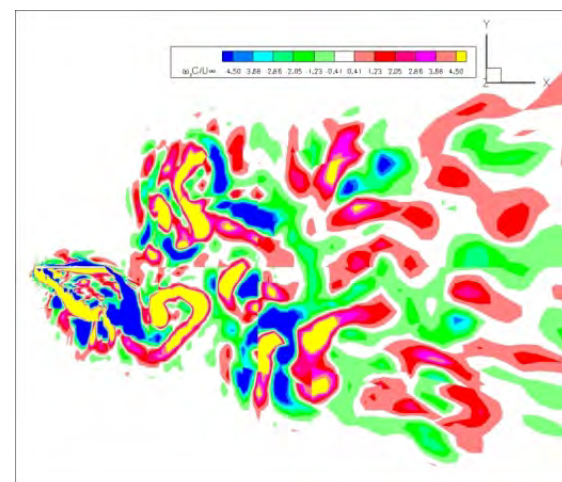
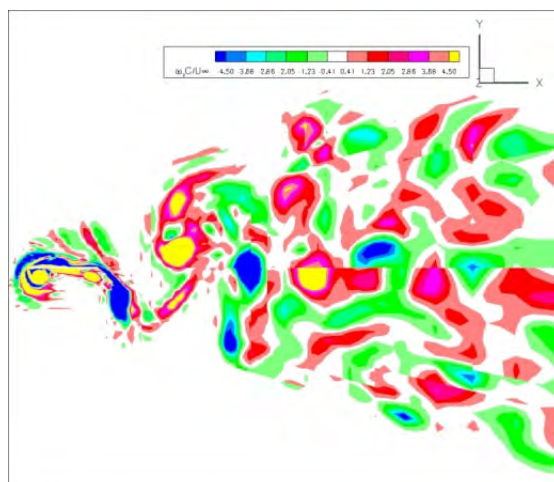
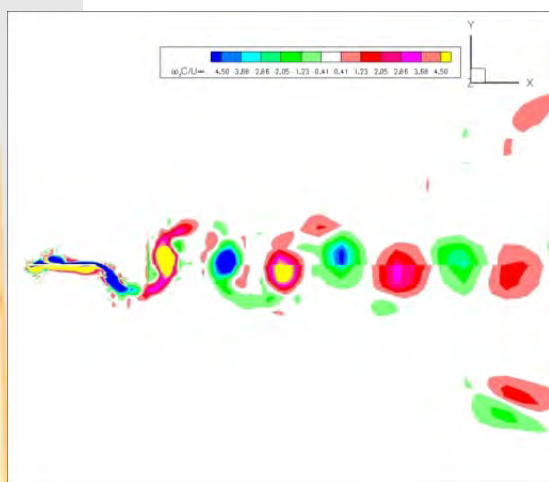
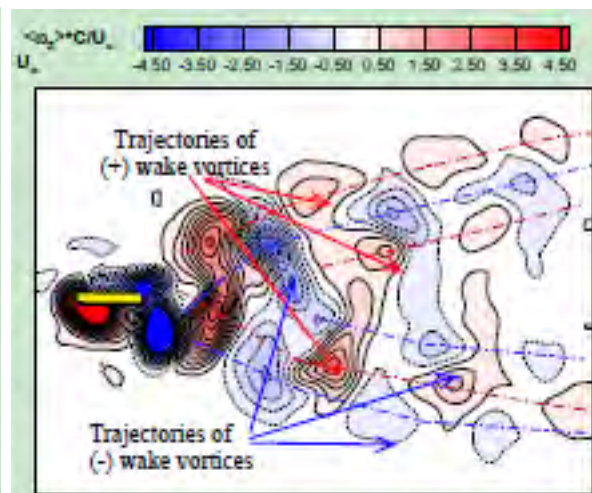
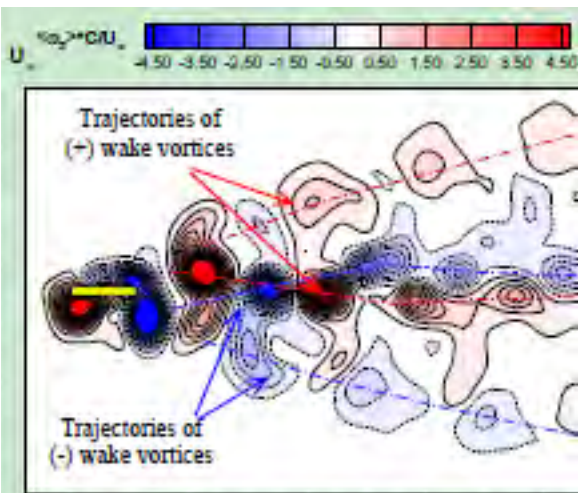
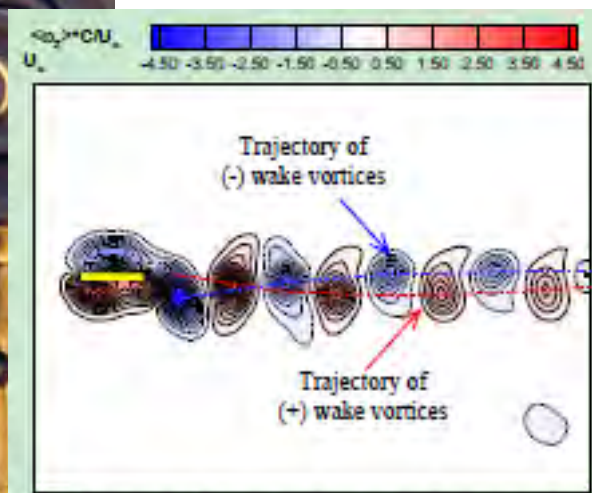
$$\bar{C}_T = 0.012$$



Iso-surfaces of Q, colored by
streamwise velocity



Comparison with Experiment (Hu et al)



50%

75%

Wingtip

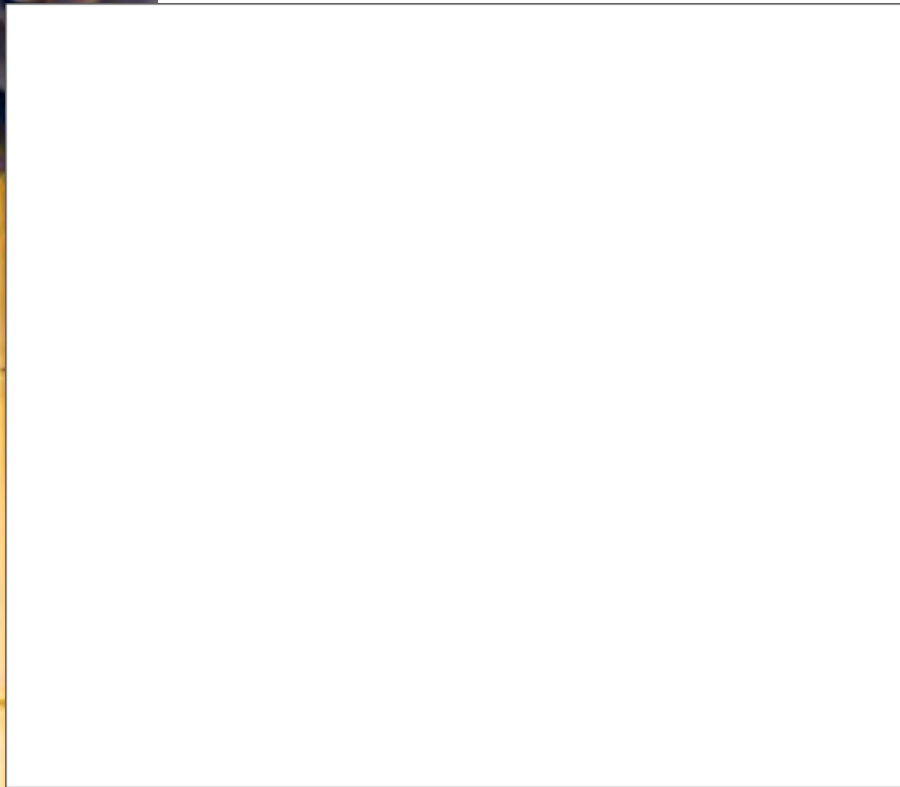
span

Instantaneous
Vorticity Field



Simulation of Flapping and Pitching Motions

$Re=1200$, $k=4.5$, $St=0.33$, Motion to maximize thrust based on Anderson et al, JFM (1998) vol. 360, pp. 41–72



Dynamic Mesh

30x larger than without pitch

Iso-surfaces of Q colored by streamwise velocity



Remaining Challenges in High-Order Methods

- Low-memory, efficient time integration/iterative solution approaches, and efficient solution algorithms for highly clustered viscous meshes
 - Memory to store the element Jacobian matrix proportional to k^6
- High-order grid generation, highly clustered curved meshes near wall
- Error estimates and solution-based hp-adaptations
- Shock capturing – to preserve accuracy in smooth regions, convergent and parameter-free



Summary

- Gave a brief introduction to high-order methods and why they are useful
- Presented several discontinuous high-order methods as the extension of the Godunov method to higher order accuracy
- Demonstrated the high-order methods with several applications
 - Computation of transitional flow and flow control
 - Bio-inspired flows
- Identified remaining challenges that intensive research efforts are needed



Acknowledgements

- Support from AFOSR, Navy, DOE, NSF, DARPA, NASA, NVIDIA and ISU
- Group members: T. Haga, H. Gao, Y. Zhou, M. Yu, V. Vikas, Yi Li, L. Shi, Yanan Li, C. Zhou